Reverse breakdown and light-emission patterns studied in Si PureB SPADs

Max Krakers[1*], T. Kneževic[1,2], and L.K. Nanver[1,3]

[1] MESA+ Institute for Nanotechnology, University of Twente, Enschede, The Netherlands
[2]Micro and Nano Electronics Laboratory, Faculty of Electrical Engineering and Computing , University of Zagreb, Croatia
[3]Dept. Mechanical and Manufacturing Engineering, Aalborg University, Aalborg, Denmark
[*]m.krakers@utwente.nl

***Abstract* – The relationship between light-emission patterns from silicon avalanche-mode light-emitting diodes (AMLEDs), and avalanche breakdown was investigated using photodiodes fabricated in pure boron (PureB) technology. The quality of the diodes ranged from high-quality, low dark-current devices with abrupt breakdown characteristics that were suitable for operation as single-photon avalanche diodes (SPADs), to diodes with gradually increasing reverse currents before actual breakdown. The reverse *I-V* characteristics were measured and correlated to light-emission data obtained simultaneously using a PureB photodetector, and inspected using a camera with which distinct emission patterns could be identified. When increasing the voltage far past breakdown, light emission invariably becomes dominant at the photodiode periphery. Based on the examination of a large variety of anode geometries, it is concluded that the most efficient light emission per consumed power is achieved with defect-free narrow-anode diodes that also are applicable as low-dark-count-rate SPADs.**

Keywords – Single-photon avalanche diode (SPAD); optocoupler; silicon; pure boron; avalanche breakdown; defects; light-emitting diode (LED); avalanche-mode LEDs

I. INTRODUCTION

High speed optical interconnects are an attractive option for increasing data transmission speeds in CMOS circuits. Ideally this should be realised using silicon (Si) diodes to exploit established CMOS fabrication facilities. Several reports have shown that using avalanche-mode light-emitting diodes (AMLEDs) rather than more commonly used forward-mode LEDs (FMLEDs) could be of advantage [1]–[5], due to the high modulation speed of AMLEDS [6] and the large overlap between the emission spectrum of AMLEDS and the spectral sensitivity of Si photodiodes (PD) [2], [5]. Recent work shows that optocouplers integrated in CMOS can be realised using a PureB AMLED and a PureB SPAD pair. [7], [8].The high photon-sensitivity of single photon avalanche diodes (SPADs) has also meant that they are gaining ground as high-resolution imaging arrays for medical applications [9] and as detectors of automotive LIDAR systems [10]. In [8] a pulse position modulation scheme was used to analyse the data transmission capabilities of the PureB AMLEDs. Some of the results of this analysis are shown in Fig. 1. It was concluded that for low bit-error rates, defect-assisted breakdown of the diode was an advantage. Since large devices had a high probability of containing defects, these performed better in this respect. In [11] the consequences of incorporating defects in AMLEDs was studied with respect to the steady-state light emission efficiency which is defined as detected photocurrent per consumed LED power. In the present paper a more detailed investigation is presented. To this end the effect of defects, doping, and geometry on avalanche breakdown, detected photocurrent, and emission patterns were recorded and analysed.

This work was supported by the Croatian Science Foundation under the project IP-2018-01-5296

II. EXPERIMENTAL METHODS

A. Device Fabrication

Devices were fabricated on (100) silicon wafers as shown in Fig. 2. As described in more detail in [11] 3 different cathode contacting regions were implemented. On p-type substrates the anode was placed in an n-type region grown eptiaxially on an n^+-buried layer, which was contacted by implanting n^+ plugs to reduce series resistance

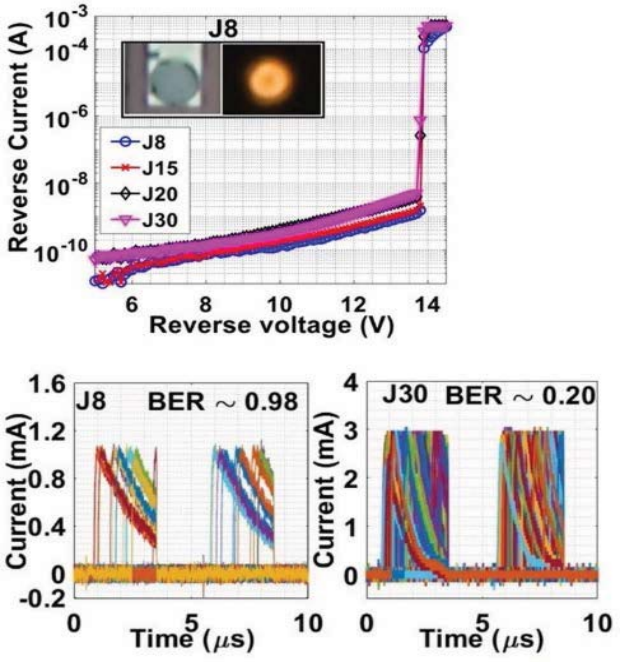

Figure 1. Results presented in [8]. Top: *I-V* characteristics of circular PureB AMLEDs with diameters of 8 µm, 15 µm, 20 µm, and 30 µm. The inset shows a micrograph of the device in the "on" and "off" state. Bottom: Transient waveforms of I_{AMLED} for 8 µm and 30 µm devices while they were biased at −17.6 V. Showing that 8 µm have an unacceptably high BER and that larger 30 µm devices have a far lower BER.

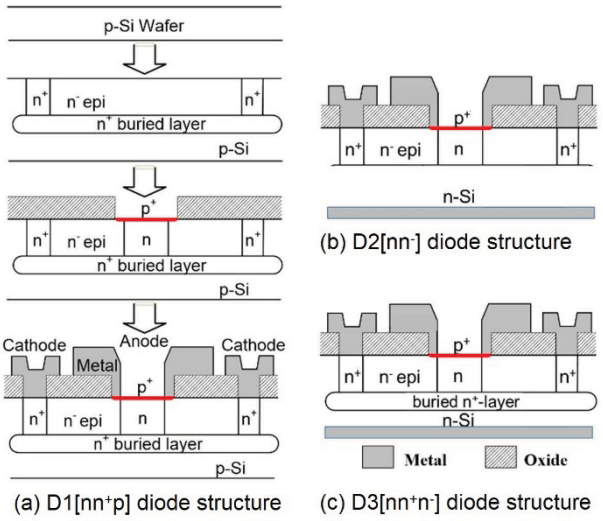

Figure 2. The diode structure and basic process flow for diodes with a buried n^+ layer on p-type and n-type silicon, and diodes without a buried n^+ layer on n-type silicon. Taken from [11].

(Fig. 2a). This design was also processed on n-type wafers where contacting was performed from the back of the wafer (Figs. 2b and 2c). Some of these devices were also fabricated without the n^+ buried layer (Fig. 2b). In the following the 3 device types will be referred to as the D1[nn^+p], D2[nn^-], and D3[nn^+n^-] diode structures, respectively. In all devices an n-enrichment region was formed by implanting phosphorus through 30 nm thermally grown silicon oxide to set the breakdown voltage (V_{br}) in the central region of the anode. The P^+ implantation was performed at 40 keV to a dose of $n = 1 \times 10^{12}$ cm^{-2}, 3.5×10^{12} cm^{-2}, 6×10^{12} cm^{-2} or 8.5×10^{12} cm^{-2}, all followed by an implant at 300 keV to a dose of 5×10^{12} cm^{-2}.The anode regions were defined by etching windows in the oxide surface isolation and depositing PureB to a layer thickness of approximately 3 nm following the process described in [12]. The layer was deposited at 700°C and driven in for 1 min at 850°C. The resulting surface doping created a junction with a thickness of approximately 15 nm with a sheet resistance in the p-type region of 1.7 kΩ/sq. To complete the devices, aluminium layers were deposited on both sides of the wafer and patterned to form electrodes to contact the anode perimeter and the cathode.

An overview of the emission characteristics of the devices was provided in [11], where it was found that devices belonging to the same type, D1[nn^+p], D2[nn^-] or D3[nn^+n^-], displayed approximately the same rate of increase of light emission with increasing LED current, I_{LED}, or increasing LED power, P_{LED}, independent of geometry. Selected results of this paper are listed in Tables I and II, where the photocurrent of a sensitive photodetector (PD) [13], I_{PD}, is a measure for the light emission as determined with the setup A described in Section II.B.

B. Emission Measurements

The emissions were investigated using two different experimental setups as shown in Fig. 3. In setup A, light-emission from the PureB LED being tested is monitored by measuring the light-induced current in a large highly-sensitive photodetector (PD) [13] mounted on the objective of a Cascade Microtech probe-station microscope while the LED was being probed and biased on-wafer. The diode voltage was swept from −0.1 V to −20 V (or −18 V) and simultaneously the PD current was recorded. As these measurements were conducted simultaneously, a direct comparison between features in the *I-V* curve and the PD current was possible. Using the same setup, forward *I-V* curves for sweeps from 0 V to 2.5 V and the concomitant LED emissions were also obtained. All measurements were conducted using a shroud and a foam seal to prevent light pollution around the detector. Before and after every sweep, the dark current was measured. These dark current measurements served as an indicator of the quality of the optical shield and were also a measure of how the ambient light/temperature changed during the day. To extract the I_{PD}

TABLE I. THE SLOPE OF $I_{PD}(I_{LED})$ AND THE SLOPE OF $I_{PD}(P_{LED})$ FOR FORWARD MODE OPERATION. ADAPTED FROM [11]

Diode type	n (atoms-cm^2)	Average $\lvert\Delta I_{PD}/\Delta I_{LED}\rvert$ ($\times 10^{-10}$)	Average $\lvert\Delta I_{PD}/\Delta P_{LED}\rvert$ ($\times 10^{-10}$ V^{-1})
D1[nn^+p^-]	1×10^{12}	88	36
D1[nn^+p^-]	6×10^{12}	96	41
D2[nn^-]	1×10^{12}	860	130
D3[nn^+n^-]	1×10^{12}	170	130

TABLE II. THE SLOPE OF $I_{PD}(I_{LED})$ AND THE SLOPE OF $I_{PD}(P_{LED})$ FOR AVALANCHE MODE OPERATION. ADAPTED FROM [11]

Diode type	n (atoms-cm^2)	Average $\lvert\Delta I_{PD}/\Delta I_{LED}\rvert$ ($\times 10^{-10}$)	Average $\lvert\Delta I_{PD}/\Delta P_{LED}\rvert$ ($\times 10^{-10}$ V^{-1})
D1[nn^+p^-]	1×10^{12}	176	10
D1[nn^+p^-]	6×10^{12}	183	9
D2[nn^-]	1×10^{12}	235	9
D3[nn^+n^-]	1×10^{12}	15	7

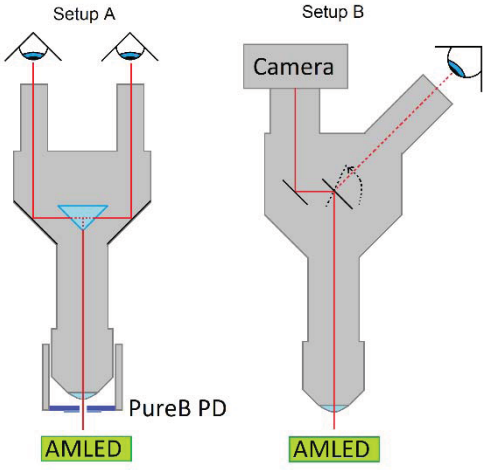

Figure 3. Two setups used for measuring PureB AMLEDs. Setup A (left) is used to obtain quantitative emission data using a highly sensitive detector mounted on a microscope objective. Setup B (right) was used to record images of the emission patterns.

from the PD current, the first four data points close to 0 V biasing were assumed to have been recorded under dark conditions. This was justifiable as the LEDs did not emit light before much higher bias voltages. The mean of these four data points was subtracted from the PD current to obtain the I_{PD}.

Setup B was used to record the emission patterns in AM by using a NIKON digital camera mounted in the optical path of the probe-station microscope, as shown in Fig 3. Images were taken using a 20× magnification and a 20 s exposure time. All electrical measurements were conducted at room temperature, using a Keithley semiconductor parameter analyser equipped with Source-Measurement-Units (SMU) and pre-amplifiers. Using these methods, a large number of PureB devices with varying sizes, geometries, and doping concentrations were investigated.

III. Results and Discussion

In Fig. 4 the reverse *I-V* curves and photocurrents are shown for circular devices of type D1[n$^+$np]. In all the devices, avalanche breakdown occurred close to the breakdown voltage set by the doping level of the n-enhancement region. However, larger devices show an earlier jump in the current level around −7 V. From Fig. 4 it is clear that such jumps are associated with an increase in photocurrent. This was also correlated to the appearance of light emission spots that could be observed with the camera for all the D1[n$^+$np] devices. A selection of these emission patterns are displayed in Fig. 5. Reverse *I-V* curves of the same diodes are shown in Fig. 6 and confirm that the increase in current around −7 V results in light emission spots. Observed current increases are expected to be defect-related avalanching events. This is supported by the reproducibility of both the *I-V* curves and emission patterns. The light emission patterns did not change upon repeated measurements, 9 of which were performed in total.

The behaviour of the 1-µm-diameter diode of Figs. 5 and 6 deviated from that of the larger diodes. Light emission from this small diode is registered by the camera but not by the PD. One explanation for this might be that non-sustained avalanching is occurring near the

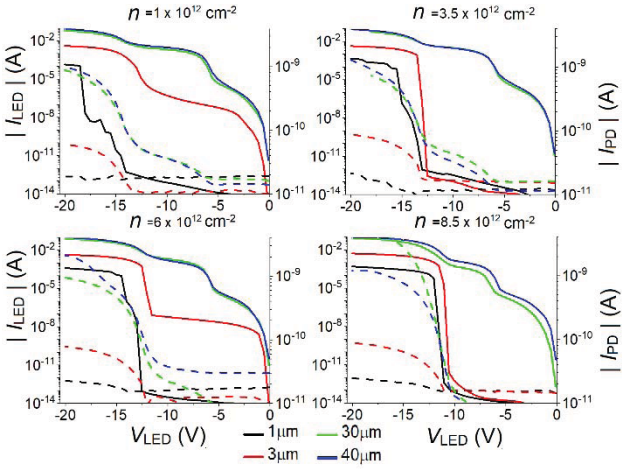

Figure 4. The reverse *I-V* curves around the breakdown voltage (solid) and the detected photocurrent (dashed) at four different doping concentrations for circular D1[n$^+$np] diodes with 4 different sizes.

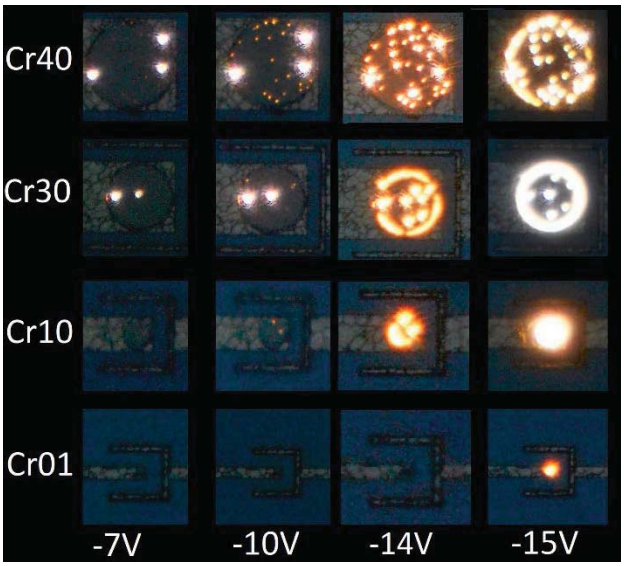

Figure 5. Light emission patterns showing 40-µm, 30-µm, 10-µm and 1-µm-diameter D1[n$^+$np] diodes with $n = 10^{12}$.cm^{-2}. All images were collected using a 20 second exposure time with brightness corrected to make small features visible.

breakdown voltage which can be seen in Figs. 4 and 6 as irregular *I-V* behaviour just past the V_{br}. Therefore the light emission is not continuous but still detected by the camera due to the long exposure time. From Fig. 4 it is also evident that increasing the doping stabilises the avalanche breakdown and results in a "fully-on" AMLED.

While Figs. 4, 5 and 6 give proof that large circular devices start emitting light at lower voltages than smaller devices where the probability of a defect is smaller, earlier reports [11] have suggested that introducing defects does not increase the emission efficiency. This is supported by Figs. 7 and 9 where the larger devices are seen to emit more light, but without any significant increase in efficiency. Moreover, in Fig. 9 the relationship between I_{PD} and the consumed LED power underlines that neither doping nor geometry have a strong effect on the emission efficiency. Instead there is a strong dependence of the light emission on the LED current both in forward-mode (FM) and avalanche-mode (AM) operation.

All the above measurements where performed on D1[nn$^+$p] devices that had complete diode isolation with

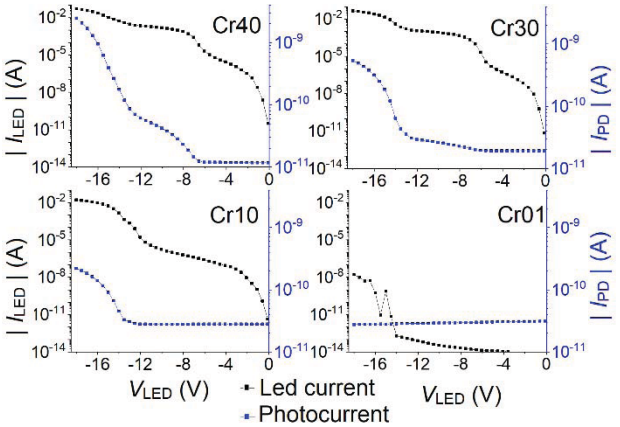

Figure 6. The reverse *I-V* characteristics and detected photocurrents for the specific diodes which were used during the light-emission measurements shown in Fig. 5.

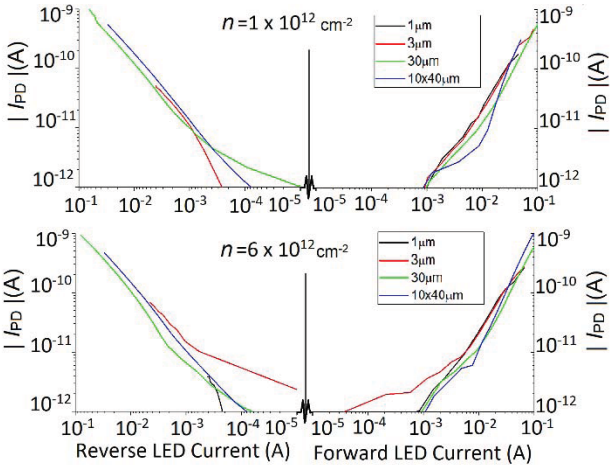

Figure 7. Photocurrent as a function of LED current for 4 D1[nn$^+$p] type diode, 3 with circular geometry with diameters 1 μm, 3 μm and 30 μm, and one with a rectangular area of 10 × 40 μm^2.

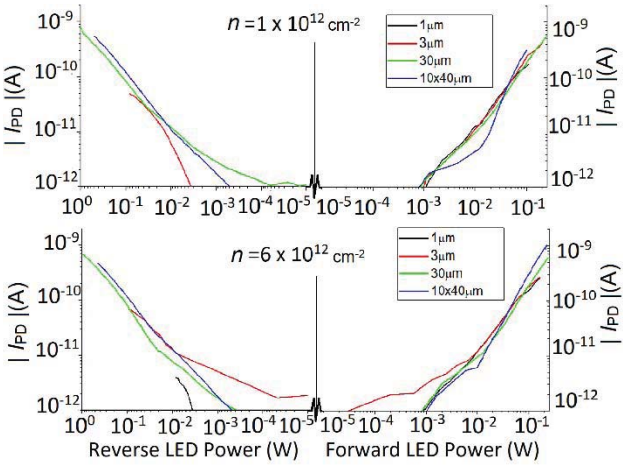

Figure 9. Photocurrent as a function of consumed LED power for 4 D1[nn$^+$p] type diode, 3 with circular geometry with diameters 1 μm, 3 μm and 30 μm, and one with a rectangular area of 10 × 40 μm^2.

buried n$^+$ layer on a p-type wafer. The same measurements were repeated on D2[nn$^-$] and D3[nn$^+$n$^-$] devices that were not isolated but placed on n-type wafers with (D3[nn$^+$n$^-$]) and without (D2[nn$^-$]) a buried layer. An overview of the results of these measurements is shown in Figs. 8 and 10. In Fig. 8 the relation between photocurrent and LED current/power is shown. While this again shows that doping has no strong influence on the light emission, it also shows that D2[nn$^-$] devices with a V_{br} = −14 V are much more efficient in FM than D3[nn$^+$n$^-$] devices with V_{br} = −7V. This is due to the larger spreading of holes injected from the anode into the substrate when the n$^+$-buried layer is omitted.

While it is clear that D2[nn$^-$] diodes in forward emit more light at lower currents than D3[nn$^+$n$^-$] diodes, the *I-V* curves in Fig. 10 show that in reverse D3[nn$^+$n$^-$] devices start emitting light at a lower voltage. Furthermore, the emission pattern of D3[nn$^+$n$^-$] diodes display emission spots comparable to the emission patterns seen in Fig. 5. This supports the earlier proposal that the emission spots are due to defect-related breakdown. In contrast, D2[nn$^-$] diodes exhibit emission rings at the diode perimeter with no spots appearing in the devices. This fits the earlier conclusion that a sharp breakdown at the voltage set by the

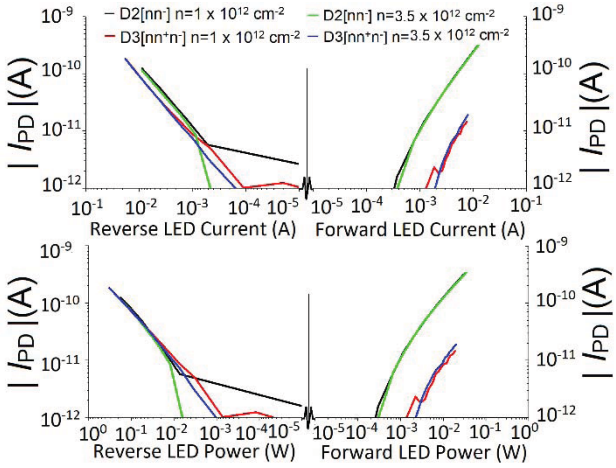

Figure 8. Photocurrent as a function of LED current (top) and consumed LED power (bottom) for circular D2[nn$^-$] and D3[nn$^+$n$^-$] diodes with a diameter of 15 μm.

enhancement doping will be associated with a emission pattern without spots.

While Fig. 8 does show that the emission efficiency of D2[nn$^-$] devices is higher than that of D3[nn$^+$n$^-$] devices in FM mode, it does not indicate any clear advantage during AM operation. In order to conclusively determine whether or not defect rich devices could be more efficient, the photocurrent versus AMLED power of a D2[nn$^-$] and a D3[nn$^+$n$^-$] device are plotted in Fig. 11. Except for the presence of the buried n$^+$ layer the devices are identical, having the same doping concentration and the same geometry. Narrow rectangular devices with an area defined by gate length, *L*, and gate width, *W*, of 2 μm × 20 μm were used to minimise the area that does not contribute to the emissions. Fig. 11 clearly demonstrates that the D2[nn$^-$] devices with a V_{br} = −14 V are more power efficient during both FM and AM operation. During AM operation the trend is most evident in the low power range up to 50 mW.

The effect of device area on the emission efficiency of rectangular D2[nn$^-$] and D3[nn$^+$n] devices is shown in Fig. 12. Here, the detected LED currents and photocurrents are shown as a function of *L* for two different voltages during

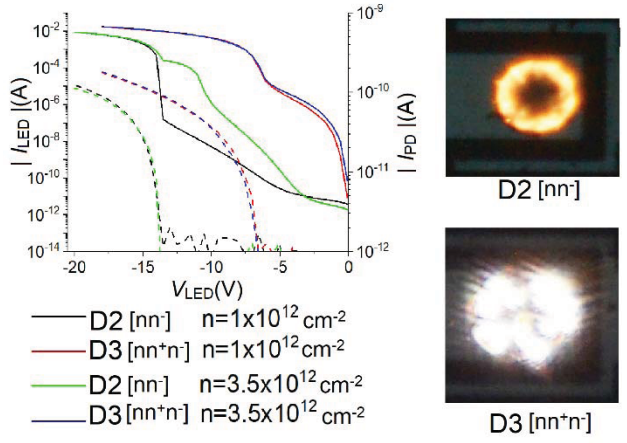

Figure 10. Left: the reverse *I-V* characteristics and detected photocurrents for circular D2[nn$^-$] and D3[nn$^+$n$^-$] diodes showing I_{LED} (solid) and I_{PD}(dashed). Right: Emission patterns of circular D2[nn$^-$] and D3[nn$^+$n$^-$] diodes with a diameter of 15 μm

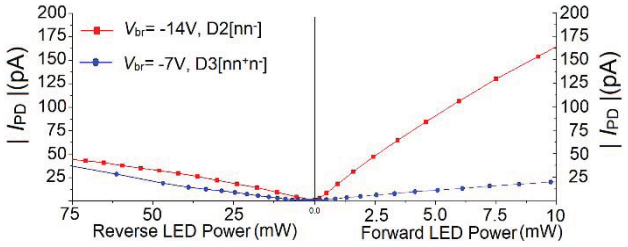

Figure 11. A comparison between D2[nn$^-$] and D3[nn$^+$n$^-$] diodes, showing the photocurrent as a function of consumed LED power. Both diodes had a rectangular geometry of 2 µm × 20 µm.

either AM or FM operation. Again, it shows that D2[nn$^-$] devices are far more efficient during FM operation with considerably higher ratio between I_{PD}/I_{LED} than D3[nn$^+$n] devices of the same size and voltage. However, both currents show no evident increase with device area since I_{LED} is dominated by the series resistance through the substrate [11]. In reverse the I_{LED} did increase with device area but the rate of increase was significantly attenuated already for 4 µm gate lengths. This could be correlated to the formation of light emission rings for the 14 V devices (D2[nn$^-$]) that indicate a strong current crowding at the anode perimeter, which was related to the sheet resistance of the anode region.

The perimeter breakdown could also contribute to increased light emissions above V_{br} set by the n-enhancement implantation but is difficult to examine experimentally. The presence of a second breakdown at the perimeter of a device close to V_{br} is shown by simulations [14]. For the devices with V_{br} = −7 V (D3[nn$^+$n]) the current attenuation is equally strong, if not stronger, but can in first instance only be correlated to the appearance of light spots. These spots do increase the amount of light emitted as compared to V_{br} = −14 V devices with the same area but at the cost of more LED current. Moreover, for the narrow devices there is an approximately 20% benefit to using D2[nn$^-$] devices. This benefit decreases with increasing device area as the sheet resistance through the anode starts to dominate and bright rings are formed at the anode perimeter. For the D3[nn$^+$n] device these rings had a spotted appearance that is not seen for the D2[nn$^-$] devices.

IV. Conclusion

The presented PureB diodes when used as AMLEDs displayed stable light-emission at visible wavelengths that could be monitored quantitatively with a PureB photodetector. The emission efficiency did not display any significant dependence on anode area/geometry or the doping of the cathode enhancement region. Furthermore, the similarities between the behaviour of D1[nn$^+$p] and D2[nn$^-$] devices indicates that the device isolation does not strongly affect the emission efficiency.

The main factors that do influence emission efficiency were identified as defect concentration and series resistance. Both these cause current hogging, the former at the position of the defects and the latter at the perimeter of the device. In both cases, this effect diminishes the chance of reaching voltages over the whole device area that could lead to light emission. Therefore, to make best use of the perimeter current crowding, narrow rectangular devices are

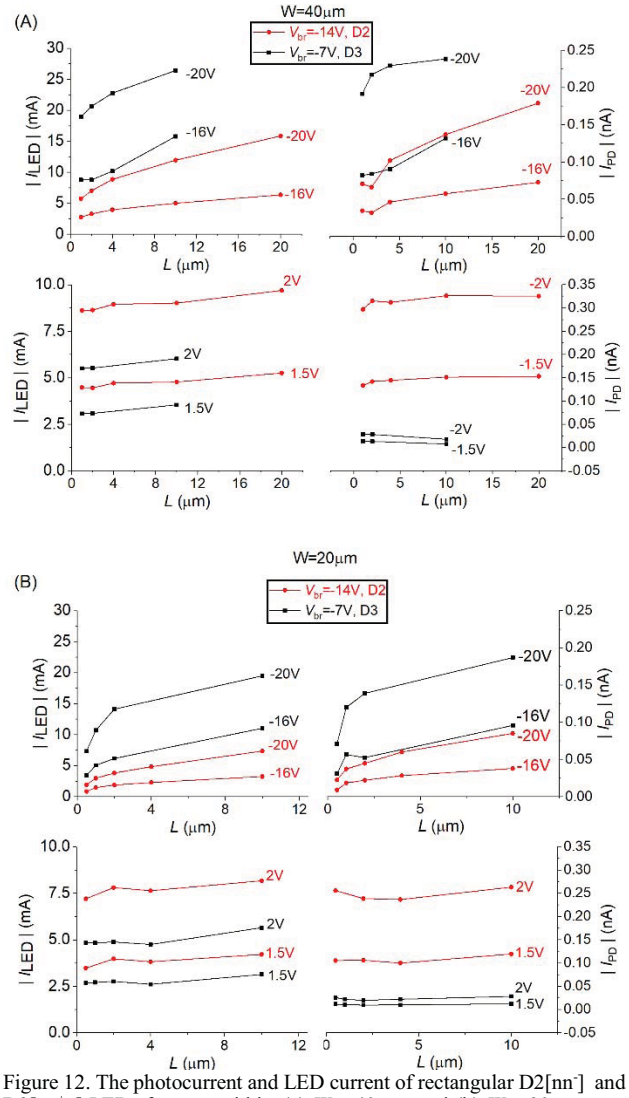

Figure 12. The photocurrent and LED current of rectangular D2[nn$^-$] and D3[nn$^+$n] LEDs for gate widths (a) W = 40 µm and (b) W = 20 µm as a function of gate length L. All devices had the same doping concentration $n = 1 \times 10^{12}$ cm^{-2}, and were measured at reverse voltages of −16 V or −20 V as well as a forward voltages of 1.5 V or 2 V.

preferable, and defects that cause local current crowding should be avoided. In [11] it was concluded that introducing defects to enhance the light emission was beneficial neither for AM nor FM operation of the diodes. From the present results it becomes clear that by introducing defects there even is a small emission penalty in AM. Therefore, the optimal device design should aim to have an as uniform as possible lateral voltage distribution over the whole light-emitting n-region of the diodes.

For the application to data transmission in on-chip optocouplers, the bit-error-rate was shown to be improved by the presence of defects to provide charge carriers for initiating avalanche events [7]. The conclusion that these extra charge carriers should preferably be supplied by sources surrounding the light-emission area rather than being placed in that area, was made in [11] because this was seen to reduce the spread in light-emission and would lead to more reproducible methods of device fabrication. From the present study it is now clear that there is a benefit for the light-emission efficiency to use defect-free SPAD-

quality diodes both for the function as SPAD detector and as the AMLED.

ACKNOWLEDGMENT

The authors would like for thank Lin Qi and the staff of the former DIMES IC-processing group for the experimental device fabrication.

REFERENCES

[1] S. Dutta, R. J. E. Hueting, V. Agarwal, and A. J. Annema, "An integrated optical link in 140 nm SOI technology," in *2016 Conference on Lasers and Electro-Optics (CLEO)*, 2016, pp. 1–2.

[2] L. W. Snyman *et al.*, "Optical sources, integrated optical detectors, and optical waveguides in standard silicon CMOS integrated circuitry," in *Silicon-based Optoelectronics II*, 2000, vol. 3953, pp. 20–37.

[3] M. du Plessis, H. Aharoni, and L. W. Snyman, "Silicon LEDs fabricated in standard VLSI technology as components for all silicon monolithic integrated optoelectronic systems," *IEEE J. Sel. Top. Quantum Electron.*, vol. 8, no. 6, pp. 1412–1419, Nov. 2002.

[4] B. Huang *et al.*, "CMOS monolithic optoelectronic integrated circuit for on-chip optical interconnection," *Opt. Commun.*, vol. 284, no. 16, pp. 3924–3927, Aug. 2011.

[5] S. Dutta, V. Agarwal, R. J. E. Hueting, J. Schmitz, and A.-J. Annema, "Monolithic optical link in silicon-on-insulator CMOS technology," *Opt. Express*, vol. 25, no. 5, pp. 5440–5456, Mar. 2017.

[6] A. Chatterjee, B. Bhuva, and R. Schrimpf, "High-speed light Modulation in avalanche breakdown mode for Si diodes," *IEEE Electron Device Lett.*, vol. 25, no. 9, pp. 628–630, Sep. 2004.

[7] V. Agarwal, S. Dutta, A. J. Annema, R. J. E. Hueting, J. Schmitz, M.J. Lee, E. Charbon, B. Nauta, "Optocoupling in CMOS," 2018 IEEE International Electron Devices Meeting (IEDM), pp. 32.1.1 - 32.1.4, 2018.

[8] V. Agarwal, A.-J. Annema, R. J. E. Hueting, S. Dutta, L. K. Nanver, and B. Nauta, "Data Transmission Capabilities of Silicon Avalanche Mode Light-Emitting Diodes," *IEEE Trans. Electron Devices*, pp. 1–8, 2018.

[9] E. Charbon, "Towards large scale CMOS single-photon detector arrays for lab-on-chip applications," *J. Phys. Appl. Phys.*, vol. 41, no. 9, p. 094010, May 2008.

[10] M. Beer, C. Thattil, J. F. Haase, J. Ruskowski, W. Brockherde, and R. Kokozinski, "SPAD-Based LiDAR Sensor in 0.35 µm Automotive CMOS with Variable Background Light Rejection," *Proceedings*, vol. 2, no. 13, p. 749, 2018.

[11] L.K. Nanver, M. Krakers, T. Knezević, A. Karavidas, I. Boturchuk, V. Agarwal, R.J.E. Hueting, S. Dutta, A.J. Annema, "Investigation of light-emission and avalanche-current mechanisms in PureB SPAD devices," Proc. SPIE 11043, Fifth Conference on Sensors, MEMS, and Electro-Optic Systems, 1104306, 2019.

[12] L. Qi, K. R. C. Mok, M. Aminian, E. Charbon, and L. K. Nanver, "Fabrication of low dark-count PureB single-photon avalanche diodes," in *2014 29th Symposium on Microelectronics Technology and Devices (SBMicro)*, 2014, pp. 1–4.

[13] A. Sakic *et al.*, "High-Efficiency Silicon Photodiode Detector for Sub-keV Electron Microscopy," *IEEE Trans. Electron Devices*, vol. 59, no. 10, pp. 2707–2714, Oct. 2012.

[14] T. Knezevic, L. K. Nanver, and T. Suligoj, "2D dark-count-rate modeling of PureB single-photon avalanche diodes in a TCAD environment," in *Physics and Simulation of Optoelectronic Devices XXVI*, San Francisco, United States, 2018, p. 55.